Vertical decoupling in Late Ordovician anoxia due to reorganization of ocean circulation

Alexandre Pohl, Zunli Lu, Wanyi Lu, Richard Stockey, Maya Elrick, Menghan Li, André Desrochers, Yanan Shen, Ruliang He, Seth Finnegan, et al.

Vertical decoupling in Late Ordovician anoxia due to reorganization of ocean circulation

Alexandre POHL[1,2*], Zunli LU[3*], Wanyi LU[3], Richard G. STOCKEY[4], Maya ELRICK[5], Menghan LI[6], André DESROCHERS[7], Yanan SHEN[6], Ruliang HE[3], Seth FINNEGAN[8], Andy RIDGWELL[1]

[1]Department of Earth and Planetary Sciences, University of California, Riverside, CA, USA

[2]Biogéosciences, UMR 6282, UBFC/CNRS, Université Bourgogne Franche-Comté, 6 boulevard Gabriel, F-21000 Dijon, France

[3]Department of Earth Sciences, Syracuse University, Syracuse, NY, USA

[4]Department of Geological Sciences, Stanford University, Stanford, CA 94305, USA

[5]Earth and Planetary Sciences, University of New Mexico, Albuquerque, NM 87131

[6]School of Earth and Space Sciences, University of Science and Technology of China, Hefei 230026, China

[7]Earth and Environmental Sciences, University of Ottawa, Ottawa ON K1N 6N5, Canada

[8]Department of Integrative Biology, University of California, Berkeley, Berkeley, CA, USA

[*]Corresponding authors

ABSTRACT

Geochemical redox proxies indicate that seafloor anoxia occurred during the latest Ordovician glacial maximum, coincident with the second pulse of the Late Ordovician mass extinction. However, expanded anoxia in a glacial climate strikingly contrasts with the warming-associated Mesozoic anoxic events, and raises questions both as to the causal mechanism of ocean deoxygenation and its relationship with extinction. Here we firstly report iodine to calcium ratio (I/Ca) data that documents increased upper-ocean oxygenation despite the concurrent expansion of seafloor anoxia. We then resolve these apparently conflicting observations as well as their relationship to global climate, by means of a series of Earth System model simulations. Applying available Late Ordovician (Hirnantian) sea-surface temperature estimates from oxygen isotope studies as constraints, alongside our I/Ca data, leads us to identify a scenario in which Hirnantian glacial conditions permit both the spread of seafloor anoxia and increased upper-ocean oxygenation. Our simulated mechanism – a reorganization of global ocean circulation, with reduced importance of northern-sourced waters and a poorer ventilated and deoxygenated deep ocean – has parallels with Pleistocene state transitions in Atlantic meridional overturning (despite a very different continental configuration), and suggests that no simple and predictable relationship between past climate state and oxygenation may exist.

The Late Ordovician mass extinction (LOME) is the first of the 'Big Five' mass extinctions[1] and was characterized by the disappearance of ~85% of marine species[2]. Extinction clustered in two apparent pulses[2] (Fig. 1) – at the beginning of the Hirnantian and near the end of the Hirnantian ('LOME 1' and 'LOME 2', respectively). LOME 1 may be related to habitat loss associated with glacioeustatically-driven sea-level changes or potentially volcanism[2–4], while the drivers responsible for LOME 2 are more debated. In the traditional time-line interpretation, LOME 2 occurred during deglaciation; extinction was then triggered by the expansion of anoxia onto the shelves during the associated sea-level rise[5]. However, studies conducted at higher stratigraphic resolution have recently challenged this model[6,7] and suggest that seafloor anoxia[7] was already well established during the latest Hirnantian glacial maximum[7,8].

The increased areal extent of seafloor anoxia, indicated by $\delta^{238}U$, coincident with glacial conditions rather than global warming, presents several apparent conundrums. Firstly, this is seemingly at odds with the well-established conceptual model for typical Mesozoic Ocean Anoxic Events which links volcanism with greenhouse-driven warming and hence the occurrence of global-scale anoxia[9]. Indeed, previous ocean biogeochemical modeling studies of Hirnantian climate have reported increased oxygenation during glaciation[10] – the expected corollary of decreased oxygenation during Mesozoic warming episodes[9]. Secondly, despite uranium isotopic evidence for expanded seafloor anoxia globally[7], most preserved stratigraphic sections, deposited at various latitudes in shelf and slope settings, record a shift to more oxic depositional facies during the Hirnantian[11]. How can deep ocean deoxygenation develop in a cold climate, and become decoupled from increased shallow marine oxygenation?

We resolve this conundrum through a series of Earth System model experiments that reveal how state transitions in large-scale ocean circulation in response to Ordovician climate change

65 can lead to a dramatic redox restructuring of the marine environment. However, we start by
66 confirming the existence of surface-to-deep redox decoupling during the latest Ordovician and
67 report the results of carbonate I/Ca measured in two Laurentian sections spanning the late Katian
68 to earliest Silurian (Rhuddanian).

69 **I/Ca data and upper-ocean oxygenation during LOME 2**

70 Bulk carbonate I/Ca (Methods) reflects changes in dissolved iodate (IO_3^-) concentration, which
71 decreases in the presence of low-oxygen water masses[12,13]. Lower I/Ca values have been
72 documented previously during Mesozoic warming events[12], providing evidence for the ocean
73 deoxygenation/warming link. Here, results obtained for two Laurentian sections (Extended Data
74 Fig. 1) show increasing mean I/Ca values from the middle segment of the Hirnantian Isotope
75 Carbon Excursion (mid HICE) to the late HICE and LOME 2 (Fig. 1, Extended Data Fig. 2). The
76 higher I/Ca values recorded in the Laurentian epicontinental seas (water depths < ~200 meters)
77 suggest that latest Ordovician cooling was contemporaneous with increased oxygenation of the
78 upper ocean, which is independently supported by the Anticosti Island organic biomarker
79 analysis of Rohrssen et al.[14] and is not easily explained as a diagenetic artifact[15,16]
80 (Supplementary Discussion and Extended Data Fig. 3). Furthermore, I/Ca values are higher at
81 Anticosti Island (Canada)[7] than at Copenhagen Canyon (USA)[17] during LOME 2 (Fig. 1). This is
82 consistent with Copenhagen Canyon being deposited in predominantly poorly oxygenated
83 offshore waters and closer to the large Laurentian oxygen minimum zone (OMZ; Extended Data
84 Fig. 1) core as well as with Fe-speciation data from Vinini Creek (Nevada) recording local
85 anoxic deep waters in an upwelling setting[18] (Fig. 1).

86 **Two models for seafloor anoxia in a cold climate**

To reconcile the various observations of increased seafloor anoxia from uranium isotopes[7], but increased upper-ocean oxygenation from I/Ca, we carry out a gridded parameter ensemble of simulations using the cGENIE Earth System model of intermediate complexity[19] configured with Ordovician continental boundary conditions and reduced (3.65 %) Ordovician solar luminosity value (Methods). We simulate a range of plausible Hirnantian climatic conditions by running the model multiple times using different atmospheric pCO_2 values (the first parameter axis in the ensemble), for which we chose a range spanning ×5 through ×24 pre-industrial (280 ppm) concentrations[20] – equivalent to 1400 to 6720 ppm.

In the ocean, it is likely that nutrient inventories were lower than modern as a consequence of reduced (compared to modern) Ordovician plant cover[21] and high sea level[22], both tending to suppress terrestrial weathering and cause lower river-nutrient input than today. We therefore also simultaneously considered a range of ocean dissolved phosphate inventories, from 0.2 to 1.0 times the present-day mean oceanic concentration ($[PO_4]$) of 2.159 μmol kg^{-1} (Fig. 2), which constitutes the 2nd parameter axis of our ensemble. We hence explore a total of 30 different combinations of pCO_2 and ocean phosphate inventory in a regular grid. All simulations were run to steady state (10,000 years) and the ensemble we focus on assumes a reasonable estimate for the Ordovician atmospheric oxygen abundance[23–25] of 8.38 % – ×0.4 the modern value of 20.95 %. Changes in the extent of seafloor anoxia simulated in response to changes in both atmospheric pCO_2 and ocean $[PO_4]$ are shown in Fig. 2.

At ×0.2 $[PO_4]$, the model Ordovician seafloor is fully oxic, regardless of the value of pCO_2 and hence climatic state (Fig. 2). As expected, the extent of seafloor anoxia (defined as benthic $[O_2] \leq 0$ μmol kg^{-1} and the presence of free sulphide (H_2S) in the model) shows a generally positive saturating relationship with increasing phosphate inventory – a direct response of the

changing bacterial oxygen demand as biological primary productivity and carbon export to the ocean interior (and the strength of the 'biological pump') increase. In contrast, we find an unexpected and highly non-linear relationship between the extent of seafloor anoxia and pCO_2, with a prominent maximum in % anoxia reached for intermediate pCO_2 values (between ×6 and ×10 CO_2) at ×0.4 [PO_4].

To identify a plausible scenario through climate-productivity space for the cooling climate leading into the Hirnantian glacial maximum (Fig. 2), we first compare modeled surface ocean temperatures with estimates from carbonate clumped isotopes[26] and $\delta^{18}O_{apatite}$[7,27] (Supplementary Results). Hirnantian climate trends are not currently known with sufficient resolution on Anticosti (or elsewhere) to precisely establish the timing of the onset of cooling leading into the late HICE glacial maximum and its relationship to the $\delta^{238}U$ and I/Ca records. We estimate the magnitude of cooling by comparing paleotemperatures from the Laframboise Member of the Ellis Bay Formation with those from the lower Ellis Bay Formation (because the Laframboise Member is interpreted as representing deglacial transgression rather than the glacial maximum[6], our estimated temperature changes are best regarded as minimal). Clumped isotopes suggest a decrease from ca. 33 °C to 29 °C, while $\delta^{18}O_{apatite}$ suggest a decrease from ca. 30 °C to 23 °C. We use these estimates to posit 2 end-member possibilities for the associated change in atmospheric pCO_2 within the model ensemble – a drop from ×24 to ×8.5 CO_2[26] (cooling Scenario #1), or a drop from ×7 to ×5 CO_2[7,27] (cooling Scenario #2).

Next, and with these 2 plausible cooling scenarios in mind, we seek to constrain pairs of simulations that are characterized by an appropriate expansion of seafloor anoxia in the cold climatic state. Mass balance modeling of the late Hirnantian negative carbonate $\delta^{238}U$ excursion at Anticosti Island[7] permits us to refine the estimate of anoxia extent by accounting for the

133 marine uranium budget[28] and indicates a shift from near-modern levels of ocean oxygenation (<
134 1 % seafloor area anoxic)[7,8], to anywhere from 3 % to 80 % total anoxic seafloor area[8] (Extended
135 Data Fig. 4; Supplementary Results). We can hence further refine our choice of model
136 simulations to pairs in which the extent of seafloor anoxia is initially (in the warm state) close to
137 modern but is substantially expanded in the cold state.
138 As illustrated in Fig. 2 (and Extended Data Fig. 5), for Scenario #1 (a pCO_2 drop from ×24 to
139 ×8.5 CO_2), we identify a pair of model experiments consistent with our criteria for anoxia
140 expansion (in this case, from ca. 0 % to 45 % of seafloor area) at a constant nutrient inventory of
141 ×0.4 [PO_4]. For #2 (pCO_2 decreasing from ×7 to ×5 CO_2), an increase in ocean phosphate is
142 required in addition to the cooling in order to trigger deep-ocean deoxygenation. We identify an
143 increase from ×0.2 to ×0.6 [PO_4] as consistent with our criteria for seafloor anoxia expansion
144 (Fig. 2, Extended Data Fig. 5). The possibility of an increase in ocean nutrient inventory is
145 supported by models and experiments suggesting that colonization of the continents by (non-)[21]
146 vascular[29] land plants could have driven a substantial increase in phosphorus weathering flux
147 during the Hirnantian[21,30]. Additional simulations run under alternative assumptions of
148 atmospheric pO_2 (Extended Data Fig. 6) reveal that these nutrient scenarios are not unique, and
149 that different combinations of pO_2 and ocean phosphate inventory may produce similar modelled
150 values of seafloor anoxia. However, the major distinction between the two scenarios remains the
151 same: cooling alone, triggers the expansion of seafloor anoxia in Scenario #1, while cooling in
152 Scenario #2 requires a simultaneous increase in ocean nutrient inventory.
153 **Reconciling shallow- and deep-marine oxygenation trends**
154 To distinguish between the 2 model scenarios, we now turn to evidence for upper-ocean
155 oxygenation changes. A key difference between Scenarios #1 and #2 is the change in the oxygen

concentrations simulated in the upper ocean (Fig. 3). In Scenario #1, oxygen concentrations in the upper ocean increase in response to climate cooling because oxygen solubility increases in colder water[10,31] while the metabolic rates of marine organisms, and thus primary productivity, decrease[32]. The rate at which particulate organic matter is degraded in the ocean interior also decreases in response to lower temperatures[32,33], with less remineralization (and hence demand in oxygen) occurring in the upper water column, leaving a relatively larger flux to be consumed at greater depths. A more efficient (deeper penetrating) biological pump also reduces the return nutrient flux to the ocean surface, further lowering primary productivity (see Methods and Supplementary Results). In contrast, for Scenario #2, upper-ocean (subsurface) oxygen concentrations decrease primarily as a consequence of a dominant nutrient inventory-driven enhancement of the biological pump which overwhelms the effects of cooling (Supplementary Results). Our I/Ca measurements then distinguish between the two scenarios and identify Scenario #1 as best capturing the overall Hirnantian ocean redox changes, with the spread of seafloor anoxia[7] paired with increased oxygenation of the upper ocean (Fig. 1).

By applying multiple data constraints to an ensemble of different realizations of Ordovician climate and marine biogeochemical cycle states, we can reconcile the divergent trends in seafloor and upper-ocean oxygenation in response to ongoing global cooling. In the model, we account for the observations as a result of a fundamental reorganization occurring in large-scale ocean circulation patterns. In the warmest ×24 CO_2 state, deep-water formation in the model predominantly occurs at the highest ocean latitudes (which in the Late Ordovician were located in the Northern Hemisphere) and ventilates much of the Ordovician seafloor with highly oxygenated waters (Fig. 4i-l). As pCO_2 is lowered through to ×8.5, seasonal sea ice appears over the North Pole (Fig. 4e-h). Seasonal freshwater fluxes associated with retreating sea-ice cover

179 locally stratify and thus stabilize the water column (Supplementary Results). This mechanism,
180 possibly strengthened by a positive feedback between reduced northwards salinity transport and
181 deep-water formation and hence overturning, leads to a shutdown of deep-water formation over
182 the North Pole. Although Southern Hemisphere overturning strengthens, this is restricted to the
183 West of the low-latitude Laurentia and Baltica continents and leaves much of the ocean floor
184 (particularly to the East of Laurentia and Baltica) poorly ventilated (Fig. 4f-g). We find support
185 for such a shift in large-scale ocean circulation occurring in response to cooling, in the higher
186 resolution MITgcm study of Pohl et al.[10]. Despite using a different continental reconstruction of
187 the Late Ordovician[34], they found a shut-down of northern-sourced, deep water in response to a
188 reduction in the solar constant and cooling, with a similar change in the pattern of global
189 overturning (Supplementary Results) and a restriction of southern-sourced oxygenation to the
190 West of Laurentia and Baltica. More idealized basin geometry (and coincidently also using
191 MITgcm) modelling also demonstrates the potential for abrupt transitions in meridional
192 overturning circulation and Rose et al.[35] find this specifically in response to the incipient growth
193 of a polar sea-ice cover. Regardless, further work using coupled climate models that can account
194 for the potential role of inter-annual variability and ocean-atmosphere modes in the state-
195 dependence of large-scale circulation patterns in the Ordovician (that we are unable to address
196 with the cGENIE model) is important and would help identify which modes of Late Ordovician
197 ocean circulation are robust (and which might be model-dependent) and how they respond to
198 climate change.

199 We suggest that a helpful analogy for better visualizing the Ordovician circulation and
200 oxygenation changes that occur in our model between ×24 and ×8.5 pCO_2 (Scenario #1), can be
201 found during the glacial-interglacial cycles of the late Pleistocene. Specifically, we note how

202 northern-sourced, deep-water production in the Atlantic decreases as climate cools (and is
203 replaced at depth by deep water sourced from the South)[36], with the potential for multiple
204 circulation states with abrupt transitions between them[35,37]. Furthermore, shallowing of the
205 Atlantic meridional overturning circulation coincides with proxy evidence for reduced
206 oxygenation at depth, despite glacial deep-ocean temperatures being colder than during
207 interglacials[38,39].

208 Finally, an important conclusion we draw from our I/Ca data and simulations is that
209 increased seafloor anoxia is, by itself, an insufficient explanation for the LOME 2. There is no
210 evidence of reduced local upper-ocean oxygenation associated with LOME 2 at Anticosti; if
211 anything there is evidence of increased oxygenation based on I/Ca at this time (Fig. 1). The
212 majority of Anticosti taxonomic last occurrences also occur above the onset of the negative
213 uranium isotope excursion[40,41], and globally many of the taxa that disappear during LOME 2
214 occurred primarily in shallow-water habitats that would have remained well oxygenated under
215 almost any reasonable global change scenario. Thus, we suggest that cooling must have
216 interacted with other factors such as changes in nutrient cycling and primary producer
217 communities[11,42], and potentially heavy metal toxicity[43], to drive the LOME 2 extinction.

218

219 **CORRESPONDING AUTHORS**

220 Correspondence and requests for materials should be addressed to A. Pohl (alexandre.pohl@u-
221 bourgogne.fr) and Z. Lu (zunlilu@syr.edu).

222 **ACKNOWLEDGMENTS**

223 

The authors thank M.J. Melchin, D. Horton and an anonymous reviewer for comments that significantly strengthened the manuscript. This project has received funding from the European Union's Horizon 2020 research and innovation programme under the Marie Sklodowska-Curie grant agreement No. 838373 (to A.P.), from NSF EAR-1349252, OCE-1232620, and OCE-1736542 (to Z.L.), from the Natural Sciences and Engineering Research Council of Canada (NSERC Discovery Grant) and NSF 17-536 (to A.D.), from the David and Lucile Packard Foundation (to S.F.), from NSF grant 1736771 and the Heising-Simons Foundation (to A.R.) and from the National Natural Science Foundation of China (41520104007, 41721002) (to Y.S. and M.L). Calculations were partly performed using HPC resources from DNUM CCUB (Centre de Calcul de l'Université de Bourgogne).

AUTHOR CONTRIBUTIONS

A.P., Z.L. S.F. and A.R. designed the study and wrote the manuscript with input from all co-authors. AP. conducted the FOAM and cGENIE experiments and led the analysis of the model results. Z.L., W.L., and R.H. carried out the I/Ca analyses. Z.L. led the analysis of the I/Ca results. R.G.S. conducted the mass balance modeling of the uranium isotope cycle.

COMPETING INTERESTS

The authors declare no competing interests.

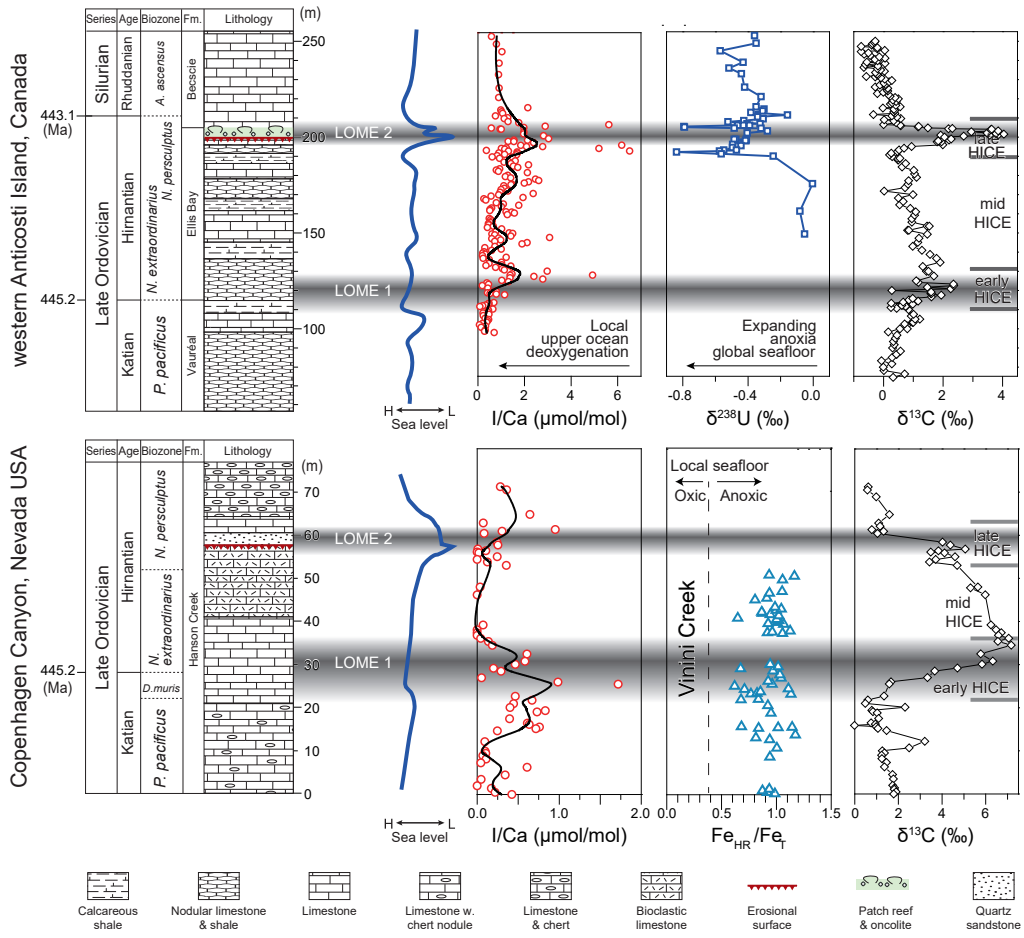

Figure 1. Stratigraphic, glacio-eustatic and geochemical records from (a) western Anticosti Island (Quebec, Canada) and (b) Copenhagen Canyon (Nevada, USA). The I/Ca curves shown with LOESS smoothing are from this study. Note the difference in scale for I/Ca between Anticosti and Copenhagen Canyon. For western Anticosti Island, stratigraphic, sea level, $\delta^{13}C$, and $\delta^{238}U$ data are from refs[6,7,44]. For Copenhagen Canyon, stratigraphic, sea level, and $\delta^{13}C$ data are from refs[17,45]; Fe-speciation data[18] are from a nearby section (Vinini Creek, Nevada). Gray shaded bands indicate the approximate stratigraphic position of LOME extinctions. Numerical ages are from ref[46]. Location of each section is shown in Fig. 3 and Supplementary Fig. 1. *HICE*: *Hirnantian Isotope Carbon Excursion*; *LOME 1 and 2*: *Late Ordovician Mass Extinction apparent pulses #1 and #2*.

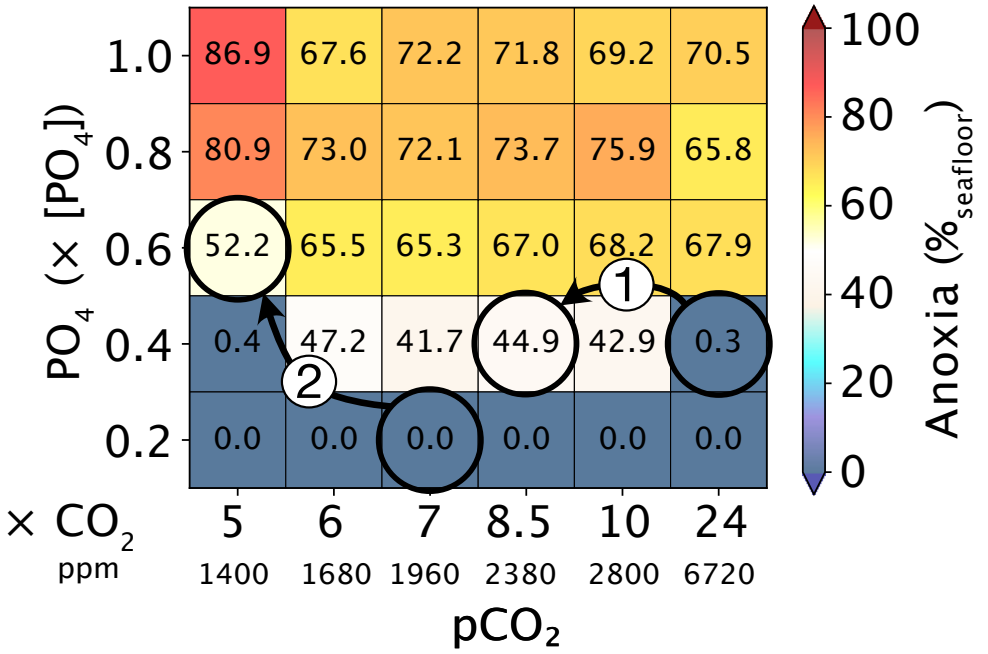

Figure 2. Simulated sensitivity of ocean anoxia to climate and marine productivity. Extent of seafloor anoxia (defined as percentage of the total seafloor area characterized by a benthic ocean $[O_2] \leq 0$ μmol kg^{-1}) as a function of both pCO_2 (x-axis) and ocean PO_4 inventory (y-axis). Values and color in each cell represent the extent of anoxia of single simulation. Arrows and labels represent Scenarios #1 and #2 discussed in the main text, selected to capture the expansion of seafloor anoxia in the latest Hirnantian glacial climate, based on temperature estimates derived respectively from clumped isotopes[26] and $\delta^{18}O_{apatite}$[7,27]. Note that pCO_2 values (x-axis) are shown in two scales: ppm and × CO_2 (times the preindustrial atmospheric concentration of 280 ppm).

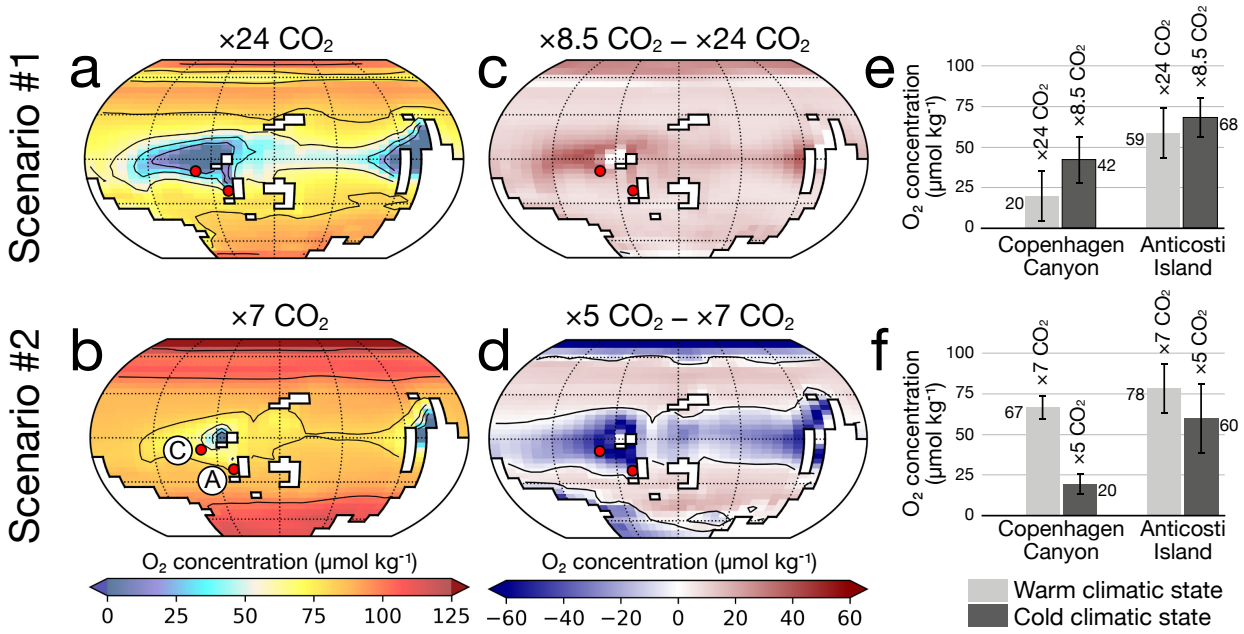

Figure 3. Upper-ocean oxygen concentrations for Scenarios #1 and #2. Upper row (a, c, e) corresponds to Scenario #1 (defined in text), bottom row (b, d, f) is Scenario #2. Left column (a, b) shows the ocean oxygen concentration simulated between 80 and 175 m water depth (i.e., the subsurface grid level in the ocean model) before cooling in Scenarios #1 (a; ×24 CO_2; ×1 CO_2 = 280 ppm) and #2 (b; ×7 CO_2). Middle column shows the impact of cooling on ocean oxygenation at the same water depth in each scenario. Emerged landmasses are shaded white and contoured with a thick black line. Red dots represent the paleo locations of Anticosti Island (A) and Copenhagen Canyon (C) (see Fig. 1). Bar plots (e, f) give, for each scenario, the oxygen concentration simulated at Anticosti and Copenhagen Canyon before (light grey) and after (dark grey) cooling. Error bars are ± 1 standard deviation, calculated based on all oceanic neighboring points in the model.

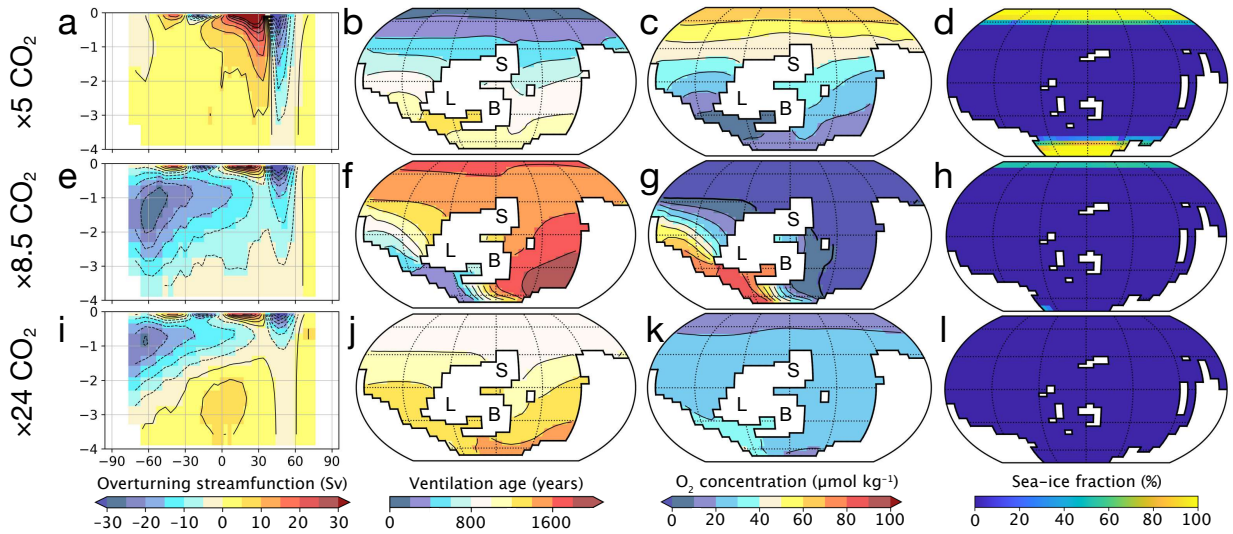

Figure 4. Ocean circulation response to cooling. Meridional overturning circulation (1st column, 1 Sv = 10^6 m^3 s^{-1}), deep-ocean ventilation age (2nd column) simulated at ca. 3900 m water depth, deep-ocean oxygen concentration (3rd column) simulated at ca. 3900 m water depth and mean annual sea-ice fraction (4th column) simulated using a pCO_2 of (a-d) ×5, (e-h) ×8.5 and (i-l) ×24 (×1 CO_2 = 280 ppm). Results shown in panels (c), (g) and (k) were obtained at ×0.4 pO_2 and ×0.4 [PO_4]. In panels (a), (e) and (i), positive (negative) values in the meridional overturning circulation represent clockwise (anticlockwise) cells. The ventilation age represents the time since a parcel of water last reached the ocean surface. *L*: *Laurentia*; *B*: *Baltica*; *S*: *Siberia*.

REFERENCES

1. Sepkoski, J. J., Bambach, R. K., Raup, D. M. & Valentine, J. W. Phanerozoic marine diversity and the fossil record. *Nature* **293**, 435–437 (1981).
2. Harper, D. A. T., Hammarlund, E. U. & Rasmussen, C. M. Ø. End Ordovician extinctions: A coincidence of causes. *Gondwana Res.* **25**, 1294–1307 (2013).
3. Saupe, E. . *et al.* Extinction intensity during Ordovician and Cenozoic glaciations explained by cooling and palaeogeography. *Nat. Geosci.* **13**, 65–70 (2019).

4. Hu, D. *et al.* Large mass-independent sulphur isotope anomalies link stratospheric volcanism to the Late Ordovician mass extinction. *Nat. Commun.* **11**, 2297 (2020).
5. Holmden, C. *et al.* Nd isotope records of late Ordovician sea-level change—Implications for glaciation frequency and global stratigraphic correlation. *Palaeogeogr. Palaeoclimatol. Palaeoecol.* **386**, 131–144 (2013).
6. Ghienne, J.-F. *et al.* A Cenozoic-style scenario for the end-Ordovician glaciation. *Nat. Commun.* **5**, 4485 (2014).
7. Bartlett, R. *et al.* Abrupt global-ocean anoxia during the Late Ordovician–early Silurian detected using uranium isotopes of marine carbonates. *Proc. Natl. Acad. Sci. U. S. A.* **115**, 5896–5901 (2018).
8. Stockey, R. G. *et al.* Persistent global marine euxinia in the early Silurian. *Nat. Commun.* **11**, 1804 (2020).
9. Jenkyns, H. C. Geochemistry of oceanic anoxic events. *Geochemistry, Geophys. Geosystems* **11**, Q03004 (2010).
10. Pohl, A., Donnadieu, Y., Le Hir, G. & Ferreira, D. The climatic significance of Late Ordovician-early Silurian black shales. *Paleoceanography* **32**, 397–423 (2017).
11. Melchin, M. J., Mitchell, C. E., Holmden, C. & Štorch, P. Environmental changes in the Late Ordovician-early Silurian: Review and new insights from black shales and nitrogen isotopes. *Geol. Soc. Am. Bull.* **125**, 1635–1670 (2013).
12. Lu, Z., Jenkyns, H. C. & Rickaby, R. E. M. Iodine to calcium ratios in marine carbonate as a paleo-redox proxy during oceanic anoxic events. *Geology* **38**, 1107–1110 (2010).
13. Lu, Z. *et al.* Oxygen depletion recorded in upper waters of the glacial Southern Ocean. *Nat. Commun.* **7**, 11146 (2016).

14. Rohrssen, M., Love, G. D., Fischer, W., Finnegan, S. & Fike, D. A. Lipid biomarkers record fundamental changes in the microbial community structure of tropical seas during the Late Ordovician Hirnantian glaciation. *Geology* **41**, 127–130 (2013).
15. Hardisty, D. S. *et al.* Perspectives on Proterozoic surface ocean redox from iodine contents in ancient and recent carbonate. *Earth Planet. Sci. Lett.* **463**, 159–170 (2017).
16. Jones, D. S. *et al.* Sea level, carbonate mineralogy, and early diagenesis controlled δ13C records in Upper Ordovician carbonates. *Geology* **48**, 194–199 (2020).
17. Hu, D. *et al.* 87Sr/86Sr evidence from the epeiric Martin Ridge Basin for enhanced carbonate weathering during the Hirnantian. *Sci. Rep.* **7**, 11348 (2017).
18. Ahm, A.-S. C., Bjerrum, C. J. & Hammarlund, E. U. Disentangling the record of diagenesis, local redox conditions, and global seawater chemistry during the latest Ordovician glaciation. *Earth Planet. Sci. Lett.* **459**, 145–156 (2017).
19. Ridgwell, A. *et al.* Marine geochemical data assimilation in an efficient Earth system model of global biogeochemical cycling. *Biogeosciences* **4**, 87–104 (2007).
20. Berner, R. A. GEOCARBSULF: A combined model for Phanerozoic atmospheric O2 and CO2. *Geochim. Cosmochim. Acta* **70**, 5653–5664 (2006).
21. Porada, P. *et al.* High potential for weathering and climate effects of non-vascular vegetation in the Late Ordovician. *Nat. Commun.* **7**, 12113 (2016).
22. Scotese, C. R. & Wright, N. PALEOMAP Paleodigital Elevation Models (PaleoDEMS) for the Phanerozoic (PALEOMAP Project, 2018). https://www.earthbyte.org/paleodem-resource- scotese-and-wright-2018/ (2018).
23. Lenton, T. M., Daines, S. J. & Mills, B. J. W. COPSE reloaded: An improved model of biogeochemical cycling over Phanerozoic time. *Earth-Science Rev.* **178**, 1–28 (2018).

24. Lu, W. *et al.* Late inception of a resiliently oxygenated upper ocean. *Science* **5**, eaar5372 (2018).
25. Sperling, E. A. *et al.* Statistical analysis of iron geochemical data suggests limited late Proterozoic oxygenation. *Nature* **523**, 451–454 (2015).
26. Finnegan, S. *et al.* The magnitude and duration of late Ordovician-early Silurian glaciation. *Science* **331**, 903–906 (2011).
27. Trotter, J. A., Williams, I. S., Barnes, C. R., Lécuyer, C. & Nicoll, R. S. Did cooling oceans trigger Ordovician biodiversification? Evidence from conodont thermometry. *Science* **321**, 550–554 (2008).
28. Zhang, F. *et al.* Uranium isotopes in marine carbonates as a global ocean paleoredox proxy: A critical review. *Geochim. Cosmochim. Acta* **287**, 27–49 (2020).
29. Steemans, P. *et al.* Origin and radiation of the earliest vascular land plants. *Science* **324**, 353 (2009).
30. Lenton, T. M., Crouch, M., Johnson, M., Pires, N. & Dolan, L. First plants cooled the Ordovician. *Nat. Geosci.* **5**, 86–89 (2012).
31. Garcia, H. E. & Gordon, L. I. Oxygen solubility in seawater: Better fitting equations. *Limnol. Oceanogr.* **37**, 1307–1312 (1992).
32. Crichton, K. A., Wilson, J. D., Ridgwell, A. & Pearson, P. N. Calibration of key temperature-dependent ocean microbial processes in the cGENIE. muffin Earth system model. *Geophys. Model Dev. Discuss.* (2020).
33. John, E. H., Wilson, J. D., Pearson, P. N. & Ridgwell, A. Temperature-dependent remineralization and carbon cycling in the warm Eocene oceans. *Palaeogeogr. Palaeoclimatol. Palaeoecol.* **413**, 158–166 (2014).

34. Torsvik, T. H. BugPlates : Linking Biogeography and Palaeogeography Software Installation. (2012).

35. Rose, B. E. J., Ferreira, D. & Marshall, J. The role of oceans and sea ice in abrupt transitions between multiple climate states. *J. Clim.* **26**, 2862–2879 (2013).

36. Adkins, J. F. The role of deep ocean circulation in setting glacial climates. *Paleoceanography* **28**, 539–561 (2013).

37. Ferreira, D., Marshall, J., Ito, T. & McGee, D. Linking Glacial-Interglacial States to Multiple Equilibria of Climate. *Geophys. Res. Lett.* **45**, 9160–9170 (2018).

38. Jaccard, S. L. & Galbraith, E. D. Large climate-driven changes of oceanic oxygen concentrations during the last deglaciation. *Nat. Geosci.* **5**, 151–156 (2012).

39. Lu, W. *et al.* I/Ca in epifaunal benthic foraminifera: A semi-quantitative proxy for bottom water oxygen in a multi-proxy compilation for glacial ocean deoxygenation. *Earth Planet. Sci. Lett.* **533**, 116055 (2020).

40. Delabroye, A. & Vecoli, M. The end-Ordovician glaciation and the Hirnantian Stage: A global review and questions about Late Ordovician event stratigraphy. *Earth-Science Rev.* **98**, 269–282 (2010).

41. McCracken, A. D. & Barnes, C. R. *Conodont biostratigraphy and paleoecology of the Ellis Bay Formation, Anticosti Island, Quebec, with special reference to Late Ordovician-Early Silurian chronostratigraphy and the systemic boundary*. *Part 2 of Geological Survey of Canada, Bulletin* vol. 329 (1981).

42. Sheets, H. D. *et al.* Graptolite community responses to global climate change and the late ordovician mass extinction. *Proc. Natl. Acad. Sci. U. S. A.* **113**, 8380–8385 (2016).

43. Vandenbroucke, T. R. A. *et al.* Metal-induced malformations in early Palaeozoic plankton

are harbingers of mass extinction. *Nat. Commun.* **6**, 1–7 (2015).

44. Desrochers, A. *et al.* A far-field record of the end Ordovician glaciation: The Ellis Bay Formation, Anticosti Island, Eastern Canada. *Palaeogeogr. Palaeoclimatol. Palaeoecol.* **296**, 248–263 (2010).

45. Finney, S. C., Berry, W. B. N., Cooper, J. D. & Ripperdan, R. L. Late Ordovician mass extinction: A new perspective from stratigraphic sections in central Nevada. *Geology* **27**, 215–218 (1999).

46. Goldman, D. *et al.* The Ordovician Period. in *Geologic Time Scale 2020* (eds. Gradstein, F. M., Ogg, J. G., Schmitz, M. D. & Ogg, G. M.) 631–694 (Elsevier, 2020). doi:10.1016/b978-0-12-824360-2.00020-6.

METHODS

Description of the model

Simulations were conducted using the Earth System model of intermediate complexity cGENIE[19] (Supplementary Methods). cGENIE is rooted in a 3D ocean circulation model, but for speed, includes only a 2D energy-moisture-balance atmospheric component plus sea-ice module. The model was configured on a 36×36 equal area grid, with 16 unevenly-spaced vertical levels in the ocean. The cycling of carbon and associated tracers in the ocean is based on a single (phosphate) nutrient limitation of biological productivity following Reinhard et al.[47] but adopts the Arrhenius-type temperature-dependent scheme for the remineralization of organic matter exported to the ocean interior of John et al.[33]. Compared to recent Earth System models of the Coupled Model Intercomparison Project phase 6 (CMIP6), the simplified climatic component of cGENIE offers a rapid model integration time, facilitating the numerous sensitivity tests required

to quantify the impact of the uncertainty in the model boundary conditions pervading deep-time studies, as well as the 10,000-year-long model simulations necessary to ensure deep-ocean equilibrium (Supplementary Results).

Description of the numerical experiments

We adopted the Hirnantian (445 Ma) continental reconstruction of Scotese and Wright[22] (Extended Data Fig. 1). In the absence of better constraints, a flat bottom ocean floor was used, which is not expected to significantly impact simulated global benthic ocean oxygenation patterns[48] (Supplementary Methods). We calculated solar luminosity at 445 Ma (1318.1 W m^{-2}) after Gough[49], and employed a null eccentricity-minimum obliquity orbital configuration, which provides an equal mean annual insolation to both hemispheres with minimum seasonal contrasts. For each different atmospheric pCO_2 assumption, we first ran the FOAM[50] general circulation model experiment for 2 kyrs using these boundary conditions (Supplementary Methods). We then derived the 2D wind speed and wind stress, and 1D zonally-averaged albedo forcing fields required by the cGENIE model, using the 'muffingen' open-source software version v0.9.20, which is assigned a DOI: 10.5281/zenodo.4615664.

cGENIE model simulations were initialized with a sea-ice free ocean and homogeneous temperature and salinity in the ocean (5 °C and 34.9 ‰, respectively). The model was then integrated for 10,000 years until equilibrium of the deep-ocean oxygen concentration. Results of the mean of the last simulated year were used for this analysis.

Materials and I/Ca methods

Samples from two Upper Ordovician sections were analyzed for I/Ca: Anticosti Island, Quebec, Canada and Copenhagen Canyon, Nevada, USA (Supplementary Methods). Rock samples were crushed and homogenized to fine powder. Around 4 mg of powdered samples were weighed and

rinsed with de-ionized water to remove soluble iodine. Nitric acid (3%) was added to dissolve carbonate. The samples were then diluted to a consistent matrix containing ~50 ppm Ca, 0.5% tertiary amine (to stabilize iodine), 5 ppb In and Cs (internal standards). The measurements were performed immediately on a quadrupole ICP-MS (Bruker M90) at Syracuse University. Iodine calibration standards were prepared daily from KIO_3 powder. The sensitivity of iodine was tuned to 80-100 kcps for a 1 ppb standard. The reference standard JCp-1 was analyzed repeatedly to monitor long-term accuracy[12,24]. The detection limit of I/Ca is on the order of 0.1 μmol mol^{-1}.

DATA AVAILABILITY

The I/Ca data can be downloaded from Zenodo (https://zenodo.org/record/5136966#.YP5vClMzbu6).

CODE AVAILABILITY

The code for the version of the 'muffin' release of the cGENIE Earth System Model used in this paper, is tagged as v0.9.20, and is assigned a DOI: 10.5281/zenodo.4618023.

Configuration files for the specific experiments presented in the paper can be found in the directory: genie-userconfigs/MS/ pohletal.NatGeo.2020. Details on the experiments, plus the command line needed to run each one, are given in the readme.txt file in that directory. All other configuration files and boundary conditions are provided as part of the code release.

A manual detailing code installation, basic model configuration, tutorials covering various aspects of model configuration and experimental design, plus results output and processing, is assigned a DOI: 10.5281/zenodo.4615662.

REFERENCES CITED IN METHODS

47. Reinhard, C. T. *et al.* Oceanic and atmospheric methane cycling in the cGEnIE Earth System model. *Geosci. Model Dev. Discuss.* 1–45 (2020).

48. Osen, A. K., Winguth, A. M. E., Winguth, C. & Scotese, C. R. Sensitivity of Late Permian climate to bathymetric features and implications for the mass extinction. *Glob. Planet. Change* **105**, 171–179 (2013).

49. Gough, D. O. Solar interior structure and luminosity variations*. *Sol. Phys.* **74**, 21–34 (1981).

50. Jacob, R. L. Low frequency variability in a simulated atmosphere-ocean system. (University of Wisconsin Madison, 1997).